Infrared magnetospectroscopy of GaAs at magnetic fields up to 150 T

S. P. Najda,* S. Takeyama, and N. Miura
Institute for Solid State Physics, University of Tokyo, Roppongi 7-22-1, Minato-ku, Tokyo 106, Japan

P. Pfeffer and W. Zawadzki
Institute of Physics, Polish Academy of Sciences, 02668 Warsaw, Poland
(Received 13 March 1989)

A study of the nonparabolic and anisotropic nature of the Γ_6 conduction band of GaAs is presented for magnetic fields up to 150 T. Spin splitting of the cyclotron resonance and donor-shifted cyclotron-resonance transitions are observed in the transmission spectra. A five-level $\mathbf{P}\cdot\mathbf{p}$ model that includes resonant and nonresonant polaron effects is developed and compared to experiment. Reasonable agreement between theory and experiment is found.

I. INTRODUCTION

Recent developments in pulsed-magnetic-field technology now enable low-temperature, high-resolution magneto-optical measurements to be performed at megagauss fields.[1] This advance permits a detailed study of the GaAs band structure at field strengths several times greater than can be obtained with continuous-magnetic-field sources. The band structure of GaAs has been of interest for many years; however, nonparabolic effects are small and hard to distinguish from polaron effects at the relatively low magnetic fields that can be obtained with superconducting, resistive, or hybrid magnets, i.e., $B < 30$ T. One of the principal advantages of using megagauss fields is that nonparabolic and anisotropic shifts are considerably enhanced at such large field strengths. In addition, polaron effects are small since the cyclotron energy (~ 130 meV) is much greater than the longitudinal-optical- (LO-) phonon energy (~ 36 meV), thus simplifying the interpretation of the data.

To a first approximation the Γ_6 band of GaAs can be regarded as isotropic and parabolic. However, interactions with neighboring bands perturb the Γ_6 band, giving rise to nonparabolic and anisotropic shifts. $\mathbf{k}\cdot\mathbf{p}$ perturbation theory has been developed to accurately determine the band curvature in the vicinity of the Γ minimum. The model is based on a semiempirical formalism using the experimentally determined energy gaps and momentum-matrix elements as input parameters. A three-level $\mathbf{k}\cdot\mathbf{p}$ model has been developed with great success to accurately describe the Γ_6 nonparabolic dispersion relationship for "narrow-gap" semiconductors, such as InSb and InAs,[2] since the valence band dominates the nonparabolic behavior of the Γ_6 band. However, for the case of a "medium-gap" semiconductor, like GaAs, this approximation is less justified since the energy difference between the fundamental gap and higher-lying conduction-band states is comparable, i.e., $E_0 \sim E_1$ (see Fig. 8). Several experiments have shown that the three-level model is not adequate for the case of GaAs and higher conduction-band states have to be considered.[3–6]

An experimental and theoretical investigation of the GaAs principal conduction band (Γ_6) is presented for magnetic fields up to 150 T. Megagauss infrared transmission experiments are performed on GaAs samples with the magnetic field oriented along the [001] and [011] crystallographic directions. It is revealed that the experimental results cannot be explained by a three-level model. A five-level $\mathbf{P}\cdot\mathbf{p}$ model is developed and compared to the megagauss data. This model considers the interaction of valence-band states, $(\Gamma_7,\Gamma_8)_v$, and higher-lying conduction-band states, $(\Gamma_7,\Gamma_8)_c$, on the Γ_6 conduction band. Nonparabolic effects rise from coupling of s-like Γ_6 states with p-type valence-band and higher-lying conduction-band states. Mixing of p-type valence-band and higher-lying conduction-band states gives rise to anisotropic shifts of the Γ_6 band. Resonant and nonresonant polaron effects are also included in the calculation. The model is fitted to low-field data, obtained from Refs. 5 and 6, then extrapolated to high field and compared to the effective-mass values obtained from the megagauss cyclotron-resonance (CR) measurements.

II. EXPERIMENTAL PROCEDURE

Formidable technical and engineering problems have to be overcome to reliably (and safely) obtain megagauss field strengths and perform magneto-optical experiments at cryogenic temperatures. The magnetic field is generated by the single-turn-coil technique. This involves the fast discharge of a 100-kJ, 40-kV capacitor bank into a 10-mm-diam copper coil. Magnetic fields up to 150 T with a rise time to full field of approximately 3 μsec can be generated by this technique. The copper coil is contained inside a large steel box to protect the optical apparatus from shrapnel and to shield the detector from any noise generated by the explosion of the coil. The absolute field strength can be determined to an accuracy of better than 2% by measuring the induced voltage in a calibrated pickup coil wound around the sample. The voltage pulse from the pickup coil is fed by optical fiber into a fast-response (nsec) 2048-word transient recorder. The transient recorder is calibrated after each shot to ensure that no spurious effects influence the field signal. In

addition, the field calibration can be verified by comparing a well-known resonance that varies linearly with field, e.g., ESR of Cr in ruby. The field homogeneity is determined to be $\pm 2\%$, 1 mm off center.

Infrared transmission experiments were performed on a 10-μm-thick GaAs sample prepared using vapor phase epitaxy, with a mobility of $\mu = 100\,000$ cm^2/V sec at 77 K and carrier concentration $n = 1.5 \times 10^{16}$ cm^3, with the magnetic field oriented along the [001] and [011] crystallographic directions. Great care was taken to orientate the sample and hold it in position along the assigned direction. The crystallographic direction was checked by x-ray crystal diffraction and was estimated to be within $\pm 1\%$ of the required direction. Tunable radiation in the range from 9.2 to 10.8 μm was provided by an externally chopped cw CO_2 laser. The CO_2 radiation was directed by a system of mirrors through the sample which is positioned at field center inside a small phenol cryostat. The transmitted radiation is incident on a high-sensitivity, fast-response (~ 1 nsec) HgCdTe detector cooled to liquid-nitrogen temperature. The detector is placed inside a doubly shielded box and the signal is transmitted optically, to reduce noise, into the second channel of the transient recorder. The sample temperature can be reduced to approximately 15 K by flowing liquid helium around the cryostat. The temperature is measured by a thermocouple placed inside the cryostat, close to the sample.

Excellent signal-to-noise levels can be achieved with this system despite the fact that the copper coil explodes after each shot. This is because the generation of the field, and therefore the data acquisition, occur several microseconds before the destruction of the coil. The explosive force is directed outward, leaving the sample and cryostat intact. A smooth parabolic field pulsed is obtained from each shot. Two similar resonance spectra are observed in the transmission signal, one corresponding to a sweep up and the other to a sweep down of the field pulse. Several shots are performed under the same experimental conditions to ensure the reproducibility of the results. It is estimated that the resolution of the pulsed field and detection system is less than 0.5 T. The spectral resolution obtained is substantially better than any previous reported fast-pulsed-field measurement and is comparable to more conventional multiple-turn, long-lifetime (msec), pulsed electromagnets. A comprehensive review of the single-turn-coil and measuring techniques is found elsewhere.[7]

III. RESULTS

Figure 1 displays typical transmission spectra for a GaAs sample with the magnetic field orientated along the [001] direction and irradiated with 130-meV, i.e., 9.2-μm, laser radiation. Cyclotron resonance can be observed at room temperature (top trace) since the condition for observing the resonance, i.e., $\omega_c \tau \gg 1$, is well satisfied at megagauss fields. As the temperature is reduced the linewidth of the resonance narrows, and two peaks are resolved at approximately 100 K. The doublet corresponds to spin splitting of the Landau-level transitions,

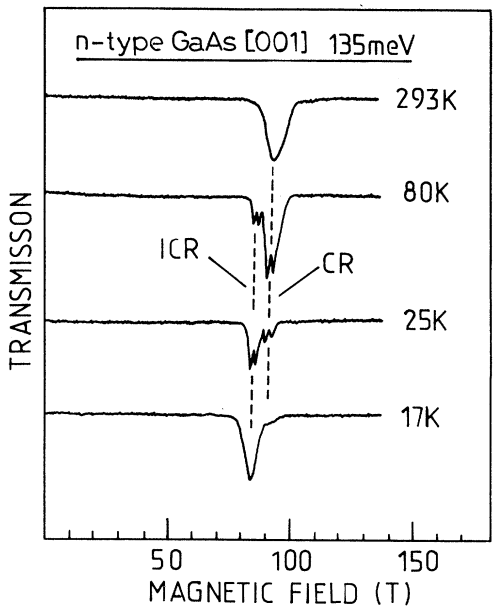

FIG. 1. The transmission spectra of GaAs[001] obtained at constant laser radiation (135 meV, 9.2 μm) for pulsed-field strengths up to 150 T and temperatures as low as 17 K is displayed. Spin-split CR ($0^{\pm} \rightarrow 1^{\pm}$) and magnetodonor transitions (ICR) $(000)^{\pm} \rightarrow (010)^{\pm}$ are observable. The resonance amplitude corresponds to approximately 20% absorption.

$0^{\pm} \rightarrow 1^{\pm}$, due to the energy dependence of the g^* factor. The calculated spin g^* value for the zeroth and first Landau level versus magnetic field intensity for two different crystal directions is shown in Fig. 2. It can be seen that in the range of magnetic fields for which the experiments have been performed, i.e., 70–100 T, an interesting situation occurs. Namely, the g^* value for the $n = 0$ level is negative for the field range studied, while the $n = 1$ level becomes positive at approximately 30 T. The difference

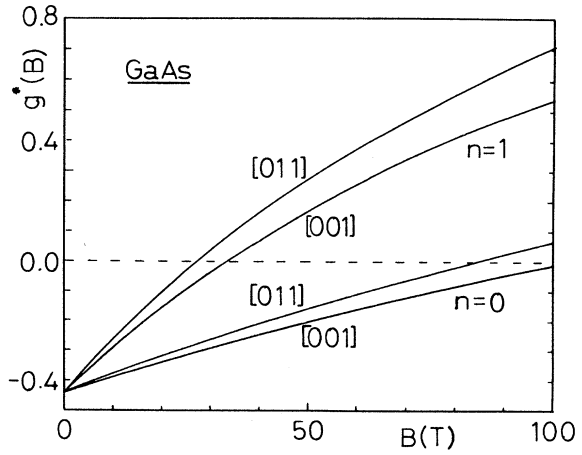

FIG. 2. Effective g^* value of GaAs for the $n = 0$ and $n = 1$ Landau levels for two different crystal directions at fields up to 100 T. At ~ 30 T the g^* value for the $n = 1$ Landau level becomes positive.

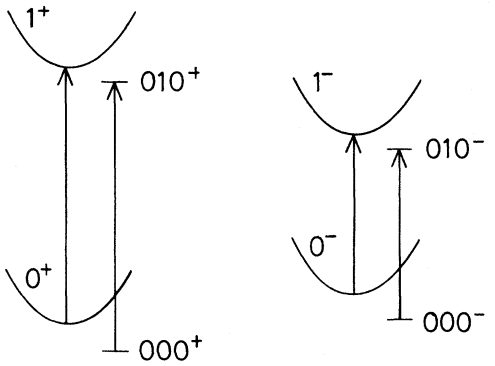

FIG. 3. The magneto-optical transitions observed in the megagauss transmission data (schematically).

in the CR energy for each spin at constant magnetic field corresponds to a splitting of the CR at fixed incident radiation. As the temperature is further reduced, additional structure at the low-field side of the CR becomes apparent due to magnetodonor transitions, i.e., $(000)^{\pm} \rightarrow (010)^{\pm}$, using high-field notation and named the impurity cyclotron resonance (ICR) or $(1S \rightarrow 2P_{+1})\uparrow\downarrow$ in low-field notation ($\uparrow\downarrow$ denotes spin up and spin down). The resulting scheme for the cyclotron resonance and impurity cyclotron resonance is shown in Fig. 3. As the temperature is further lowered, the intensity of the impurity transitions increases at the expense of the CR transition. At the lowest measurable temperature, carrier freeze-out occurs, leaving only localized impurity state transitions observable. There is no detectable shift of the transition peak positions as the temperature is reduced.

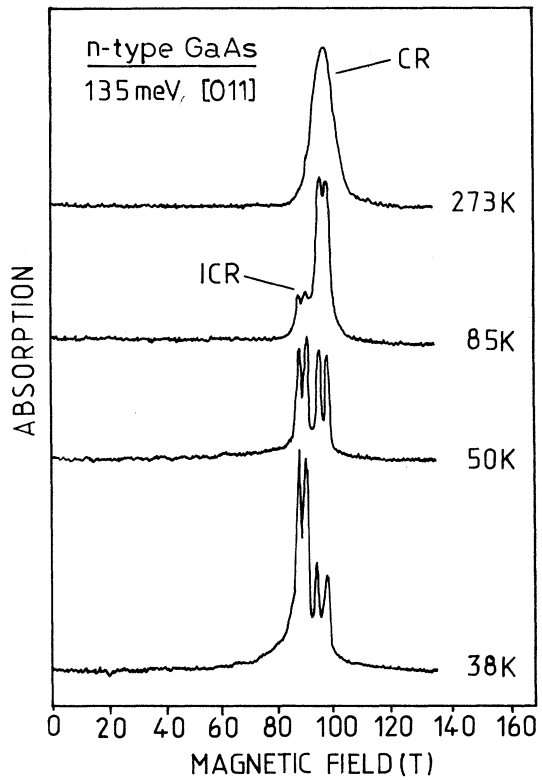

FIG. 4. Absorption of GaAs [011] at megagauss fields and constant wavelength ($\lambda = 9.2\ \mu$m). As the temperature is reduced magnetodonor transitions (ICR) are observed.

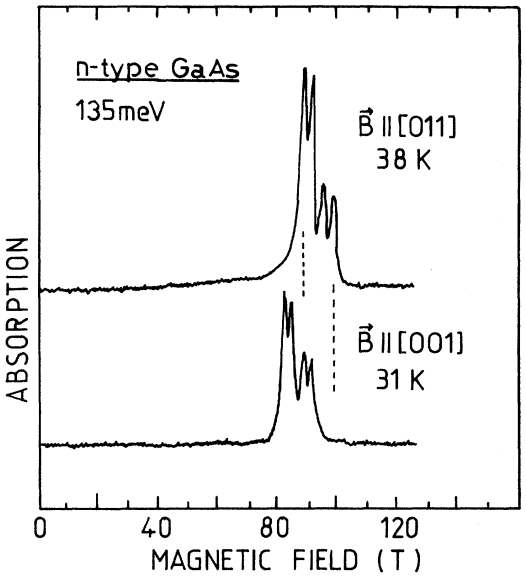

FIG. 5. A GaAs crystal irradiated with the same laser wavelength ($\lambda = 9.2\ \mu$m) at approximately constant temperature for the magnetic field oriented along the [011] (top trace) and [001] (bottom trace) crystallographic direction.

A diagram of the GaAs absorption spectra for the magnetic field orientated along the [011] crystallographic direction is shown in Fig. 4. At low temperatures spin-split CR and magnetodonor transitions are observable in a similar manner to Fig. 1. The nonsphericity of the Γ_6 band can be clearly observed by comparing spectra at the same incident wavelength and temperature, but for the magnetic field orientated along different crystallographic directions. The resonance peak positions for the [011] direction occur at fields shifted about 6% greater than for the [001] direction (Fig. 5).

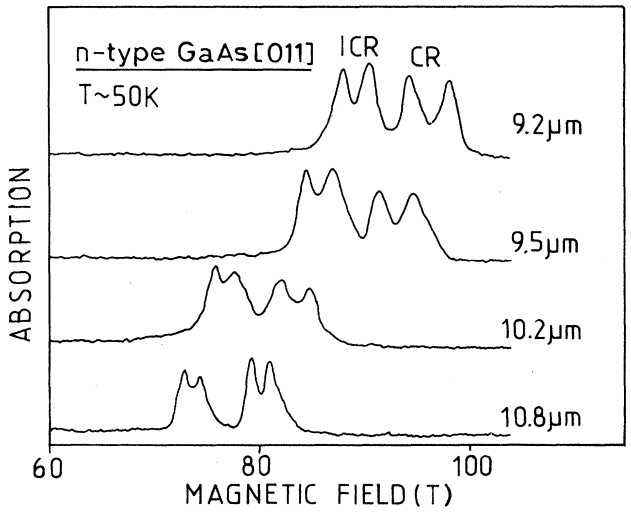

FIG. 6. The evolution of the resonance transitions as a function of wavelength at approximately constant temperature.

The absorption spectra of GaAs[001] for several different wavelengths at approximately constant temperature is shown in Fig. 6. This figure shows the high spectral resolution that can be obtained with the single-turn–coil, pulsed-field system. At the shortest incident wavelength (highest field), the resonance peaks are well resolved with a half-width at half-height of less than 1 T.

The peak positions of the ICR and the CR transitions for the [001] direction are plotted on an energy (meV) versus magnetic field diagram for several different wavelengths in Fig. 7. This diagram graphically illustrates the greatly increased spectroscopic energy range that can be achieved with the pulsed-field system, compared to continuous-field sources which are limited to field strengths below the LO-phonon energy. A three-level calculation[2] is compared to the CR results. (Values used in the calculation are $E_g = 1.51$ eV and $\Delta_0 = 0.17$ eV.) It is clear from this diagram that the three-band calculation completely underestimates the magnitude of the CR splitting and does not predict any anisotropy of the band. (The CR splitting of the three-band calculation is too small to resolve on this figure.) Nevertheless, the **B**||[001] megagauss data fit the three-level model surprisingly well (but not for **B**||[011]). It is not clear why this is the case, since low-field measurements indicate a significant deviation from the three-level model, requiring an extension of the band model to include five levels to explain the data.[5,6]

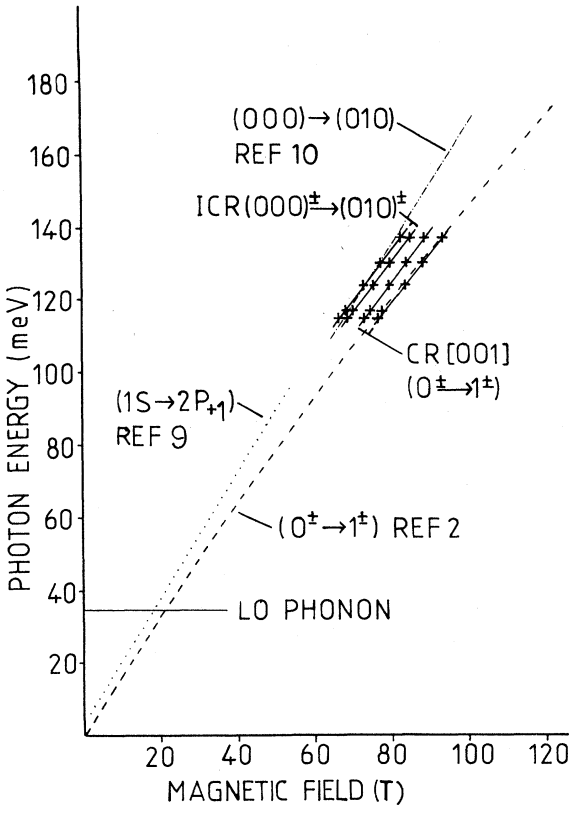

FIG. 7. The ICR and CR data for the [001] crystallographic direction compared to two theoretical models of the magneto-donor binding energy (Refs. 9 and 10) and a three-level band calculation (Ref. 2).

A value of the effective mass far from the band edge can also be determined from magnetotransport and Faraday-rotation measurements of highly doped GaAs. (It should be noted that much purer samples are used for the megagauss magneto-optical experiments.) The various effective masses obtained from the above experiments are compared to two-level and five-level models.[8] For samples with impurity concentrations up to 10^{19} cm^{-3}, the Fermi level is $\sim$200 meV above the band edge and the data are well described by the five-level model. However, for smaller impurity concentrations, so that the Fermi energy roughly corresponds to the average energy of the magneto-optical transitions, i.e, $E = \hbar\omega_c \simeq 130$ meV, the experimental effective-mass values are considerably dispersed between the calculated values derived from two-level and five-level models. The megagauss magneto-optical results fit within the range of previously obtained data.

Also included on this diagram is the donor binding energy calculated for two different magnetic field ranges. (The magnetic field range is defined by a dimensionless parameter $\gamma = \hbar\omega_c / R^*$, where $R^* = 5.7$ meV is the effective Rydberg of GaAs.) The $1S$-$2P_{+1}$ transition[9] (accurate for the low-field regime, $\gamma \sim 1$) for a shallow donor impurity attached to a parabolic band is plotted together with a high-field ($\gamma \gg 1$) calculation[10] for the (000)→(010) transition. (The values used in the calculation are $m^* = 0.0660 m_0$, $E_g = 1.15$ eV, and $\Delta_0 = 0.17$ eV.) The megagauss ICR data fit the high-field three-level magnetodonor calculation reasonably well for the case of **B**||[001] (but not for **B**||[011]). The figure demonstrates the inadequacy of existing magnetodonor calculations to explain the ICR data for the range of fields studied. An additional paper will be published concerning magnetodonors at megagauss magnetic fields. Only the free-electron data are considered further.

IV. DISCUSSION OF THE FIVE-LEVEL P·p MODEL AND COMPARISON WITH EXPERIMENT

The band structure of GaAs in the vicinity of the Γ point is considered by a five-level **P**·**p** model, taking into account the Γ_{8c}, Γ_{7c}, Γ_{6c}, Γ_{8v}, and Γ_{7v} levels at $k = 0$ (cf. Fig. 8). The **P**·**p** theory can be described as a generaliza-

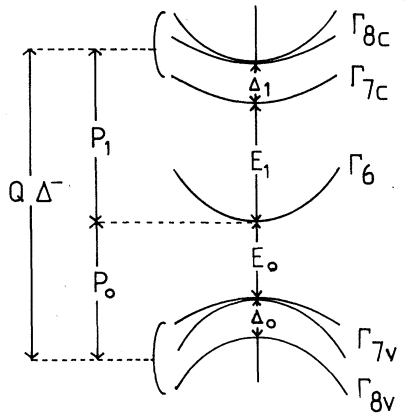

FIG. 8. The band structure of GaAs near the Γ point (schematically).

tion of the $\mathbf{k}\cdot\mathbf{p}$ scheme for the case of an electron in a periodic crystal potential subject to an externally applied magnetic field. This amounts to replacing the wave vector $\mathbf{k}$ by $\mathbf{P}=\mathbf{p}+e\,\mathbf{A}$, where $\mathbf{A}$ is the vector potential of the magnetic field, in the multiband Hamiltonian.[11] The resulting $\mathbf{P}\cdot\mathbf{p}$ equation, written in the Luttinger-Kohn representation, for the envelope functions $f_l(r)$ is

$$\sum_l \left[\left(\frac{1}{2m_0} P^2 + E_l - E \right) \delta_{l'l} + \frac{1}{m_0} \mathbf{p}_{l'l}\cdot\mathbf{P} + \mu_B \mathbf{B}\cdot\boldsymbol{\sigma}_{l'l} + H^{so}_{l'l} \right] f_l = 0 \,,$$

where indices l and l' run over the above bands, m_0 is the free-electron mass, E_l are the band-edge energies, μ_B is the Bohr magneton, σ is the Pauli spin vector, and $H^{so}_{l'l}$ are the interband matrix elements of the spin-orbit interaction.

The basis functions are chosen in such a way that they diagonalize the spin-orbit interaction within the $(\Gamma_7,\Gamma_8)_v$ and $(\Gamma_7,\Gamma_8)_c$ sets. Since the zinc-blende structure does not have inversion symmetry, an off-diagonal matrix element of the spin-orbit term between the above sets has to be included, $\Delta^- \sim \langle X^v | [\nabla V, \mathbf{p}]_y | Z^c \rangle$. (Alternatively, a more complicated basis can be chosen in which the interband spin-orbit term does not appear, but this in turn would complicate the interband momentum-matrix elements.) A value of the off-diagonal spin-orbit term, $\Delta^- = -0.061$ eV, has recently been determined from pseudopotential calculations by Gorczyca *et al.*[12] Three other interband momentum-matrix elements appear in the five-level model: $P_0 \sim \langle S|p_x|X^v\rangle$, $P_1 \sim \langle S|p_x|X^c\rangle$ and $Q \sim \langle X^v|p_y|Z^c\rangle$. The P_0 and P_1 matrices correspond to mixing of p-type valence-band and higher-lying conduction-band states, respectively, with s-type Γ_6 states, and are mainly responsible for the band nonparabolicity. The Q matrix gives rise to anisotropy of the Γ_6 band due to coupling between p-type higher-lying conduction bands with p-type valence-band states. The four momentum-matrix elements and the far-band contributions, C and C' to m_0^* and g_0^* respectively, constitute the six input parameters to the model. (The energy gaps, indicated in Fig. 8, used in the calculation are $E_0 = 1.519$ eV, $E_1 = 2.969$ eV, $\Delta_0 = 0.341$ eV, and $\Delta_1 = 0.171$ eV.) The following values of the interband matrix elements are used in the five-level model: $E_{P_0} = 27.86$ eV, $E_{P_1} = 2.361$ eV, and $E_Q = 15.56$ eV (in standard units $E_p = 2P^2/m_0$), the far-band contributions to the band-edge effective mass $C = -2.15$, and the band-edge g^* value $C' = -0.0215$. These values result in a conduction-band-edge mass $m_0^* = 0.0660 m_0$ (including a nonresonant polaron contribution, see below), and $g_0^* = -0.44$. The above parameters describe well all previous magneto-optical data taken at magnetic fields up to 24 T. (The parameters quoted in Refs. 5 and 6 are slightly different since a somewhat lower value of m_0^* is used in this case compared to Ref. 5 and a slightly larger value of Δ^- compared to Ref. 6; also polaron effects are included in the spin-doublet splitting of the CR.)

Fourteen coupled differential equations[11] are obtained for the envelope functions f_1. Since the conduction band is anisotropic, due to the appearance of the matrix element Q, solutions are found by looking for envelope functions f_1 in the form of sums of harmonic-oscillator functions rather than simple harmonic functions as is the case for the three-level model.[13] An infinite-dimensional matrix is obtained where different Landau states are coupled with Q matrix elements. The matrix is subsequently truncated and diagonalized numerically. The direction of the magnetic field with respect to the crystal axis is chosen by taking the appropriate gauge. The reference frame is rotated by aligning the new z axis along the magnetic field direction. This leaves a large part of the matrix invariant, and only the Q-dependent terms change for different field directions. A 21×21 matrix is diagonalized for $\mathbf{B}\|[001]$, and a 35×35 matrix for $\mathbf{B}\|[011]$.

Although GaAs is a weakly polar material (coupling constant $\alpha = 0.065$) and the experiments are performed at energies well beyond the longitudinal-optic-phonon energy ($\hbar\omega_L = 36.2$ meV), resonant and nonresonant polaron effects are included in the theoretical description. The nonresonant polaron contribution is important for the $\mathbf{P}\cdot\mathbf{p}$ theory since at $B = 0$ the polaron mass is given by[14]

$$\frac{m^*_{\rm pol}}{m_0^*} = \frac{1+\alpha/2}{1+\alpha/3}$$

where m_0^* is the bare effective mass. This effect must be accounted for when determining the bare mass from the experimental one, i.e., $m^*_{\rm pol}$. The $\mathbf{P}\cdot\mathbf{p}$ calculation is first performed with the "bare" parameters, and then the polaron contribution is included to obtain values to compare with experiment. The five-level model is fitted to the low-field data,[5,6] then extrapolated to high fields and

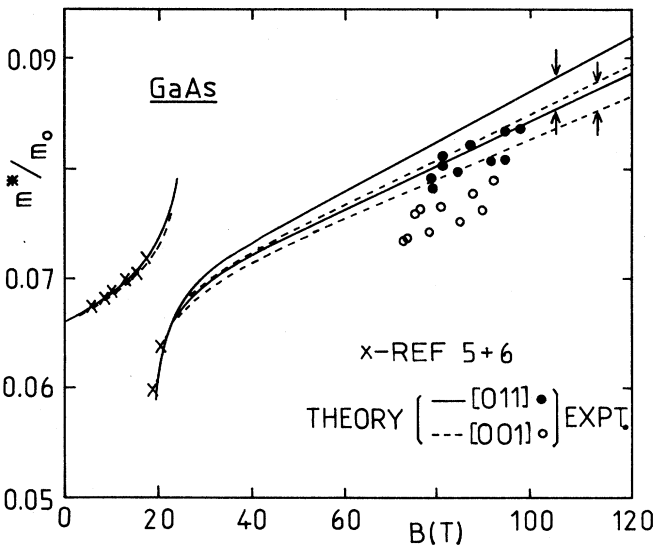

FIG. 9. The effective-mass values obtained from the five-band calculation for two crystallographic directions plotted against magnetic field (the solid and dashed lines are for the [011] and [001] crystal directions, respectively). Low-field data are provided by Sigg *et al.* (Ref. 5) and Hopkins *et al.* (Ref. 6). The solid circles are for the [011] CR data and open circles for [001] CR data.

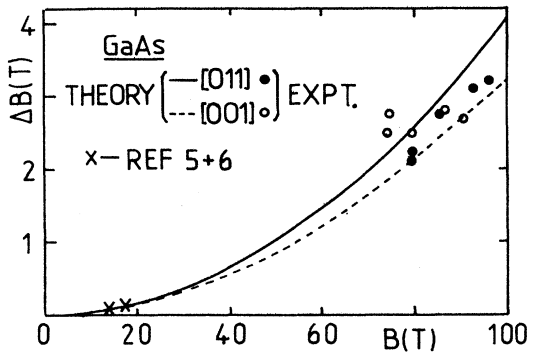

FIG. 10. CR splitting (ΔB) as a function of B for two crystal directions. The solid circles are for the [011] direction and the open circles for the [001] direction. Low-field data are from Sigg *et al.* (Ref. 5) and Hopkins *et al.* (Ref. 6).

compared to the megagauss results.

The effective mass m^* is determined from the CR by the relation

$$\omega_c = \frac{eB}{m^*} ,$$

where ω_c is the cyclotron frequency and B the resonance-field position. This value is then compared to the calculated values of m^* obtained from the five-level model in Figs. 9 and 10.

A plot of the effective mass for two spin directions versus magnetic field is shown in Fig. 9. The solid lines are the calculated m^* values for the [011] crystal direction and the dashed lines for the [001] direction. The discontinuity of the effective mass at $\sim$20 T is due to LO-phonon coupling. The effective-mass values determined from the CR data are plotted as solid circles for the [011] direction and open circles for [001]. (Magnetodonor transitions are omitted for clarity on this diagram.) The anisotropy between the two crystal directions can be clearly seen from this diagram as a $\sim$4% increase of the effective mass for the [011] direction compared to the [001] direction. The five-level model overestimates the magnitude of the nonparabolicity for both crystal directions. For the case of the [011] direction, theory overestimates the experimental mass by $\sim$4% and by $\sim$8% for the [001] direction.

Figure 10 plots the CR spin splitting, ΔB, against B for fields up to 100 T. The experimental and theoretical values of the spin-doublet splitting coincide rather well up to the highest fields. However, the experimental resolution is insufficient to observe any systematic anisotropic shift of the conduction band from the spin-split CR data.

The five-level model predicts larger masses and smaller band anisotropy than determined by the megagauss experiments. It should be mentioned that at low fields (up to 24 T) the same theory gives larger band anisotropy than observed.[5,6] The discrepancy between the high-pulsed-field and low-continuous-field measurements is not understood at present.

V. CONCLUSIONS

The megagauss transmission experiments demonstrate the high sensitivity and suitability of using ultrafast pulsed magnetic field (μsec) to study magnetodonor transitions and the band structure of semiconductors in an unexplored field regime. The GaAs megagauss CR data provide a rigorous test of the five-level $\mathbf{P}\cdot\mathbf{p}$ model which explicitly considers the perturbative influence of higher-lying conduction-band $(\Gamma_7,\Gamma_8)_c$ and valence-band states $(\Gamma_7,\Gamma_8)_v$ on the Γ_6 band. The overall agreement between theory and experiment is reasonably good considering the simple extrapolation procedure used in the calculation and the relatively inferior resolution (compared to continuous fields) of the pulsed-field measurement. However, it should be emphasized that the experimental resolution is significantly better than any previous reported fast-pulsed-field measurement. This is demonstrated by the observation, at low temperature, of magnetodonor resonances with a half-width at half-height of less than 1 T.

The agreement between theory and experimental values of the spin-doublet splitting, ΔB, is rather good. However, the precision of the pulsed-field measurements is insufficient to observe a systematic anisotropic shift of ΔB for different crystal directions; therefore, a value of the matrix element Q cannot be determined from the experiment. At megagauss field strengths the GaAs effective mass increases by more than 20% of its band-edge value and a large anisotropic shift is observed ($\sim$4% difference in the effective mass) between the [001] and [011] crystallographic directions. The five-level model overestimates the effective mass, i.e., overestimates the nonparabolicity, for both crystal directions ($\sim$4% for the [011] direction and $\sim$8% for the [001] direction), and the observed anisotropic shift is larger than predicted by theory. This is in contrast to the low-field experiments taken by Sigg *et al.*[5] and Hopkins *et al.*[6] Their data fit the five-level model well for both crystal directions; however, they measure a weaker anisotropy than calculated. It is not clear why there are discrepancies between the pulsed-high-field and low-field measurements. The deviation of the calculated and experimental effective-mass values at megagauss fields is probably due to remote higher-lying conduction-band states not being treated explicitly in the five-level model but rather included in constant terms C and C'. A more accurate high-field calculation would need to consider higher-band states more carefully.

*Present address: SNCI-CNRS, 25 avenue Des Martyrs, Boîte Postale 166X, Grenoble 38042, France.

[1]N. Miura and F. Herlach, in *Strong and Ultra Strong Magnetic Fields,* edited by F. Herlach (Springer-Verlag, Berlin, 1985), p. 247.

[2]B. Lax, J. G. Mavroides, H. J. Zeiger, and R. J. Keyes, Phys. Rev. **122**, 31 (1961).

[3]C. Hermann and C. Weisbuch, Phys. Rev. B **15**, 823 (1977).

[4]V. G. Golubev, V. I. Ivanov-Omskii, I. G. Minervin, A. V. Osutin, and D. G. Poylakov, Pis'ma Zh. Eksp. Teor. Fiz. **88**, 2052 (1985) [JETP Lett. **61**, 1214 (1985)].

[5]H. Sigg, J.A.A.J. Perenboom, P. Pfeffer, and W. Zawadzki, Solid State Commun. **61**, 685 (1987).

[6]M. A. Hopkins, R. J. Nicholas, P. Pfeffer, W. Zawadzki, D. Gauthier, J. C. Portal, and M. A. DiForte-Poisson, Semicond. Sci. Technol. **2**, 568 (1987).

[7]K. Nakao, F. Herlach, T. Goto, S. Takeyama, T. Sakakibara, and N. Miura, J. Phys. E **18**, 1018 (1985).

[8]W. Zawadzki and P. Pfeffer, in *High Magnetic Fields in Semiconductor Physics,* Vol. 71 of *Springer Series in Solid State Physics,* edited by G. Landwehr (Springer-Verlag, Berlin, 1987), p. 523.

[9]C. Aldrich and R. L. Greene, Phys. Status Solidi B **93**, 343 (1979).

[10]D. M. Larsen, J. Phys. Chem. Solids **29**, 271 (1968); also see R. Bowers and Y. Yafet, Phys. Rev. **115**, 1165 (1959).

[11]W. Zawadzki, in *Narrow Gap Semiconductors, Physics and Applications,* Vol. 133 of *Lecture Notes in Physics,* edited by W. Zawadzki (Springer-Verlag, Berlin, 1980), p. 85.

[12]I. Gorczyca, P. Pfeffer, and W. Zawadzki (unpublished).

[13]V. Evtuhov, Phys. Rev. **125**, 1869 (1962).

[14]P. Pfeffer and W. Zawadzki, Phys. Rev. B **37**, 2695 (1988).